Tribology International 161 (2021) 107052

Contents lists available at ScienceDirect

Tribology International

journal homepage: www.elsevier.com/locate/triboint

Normalising tactile friction

D.A. Sergachev [a,*], D.T.A. Matthews [a,b], E. van der Heide [a,c]

[a] Laboratory for Surface Technology and Tribology, Faculty of Engineering Technology, University of Twente, Enschede, the Netherlands
[b] Institute of Plasma, Feng Chia University, Taiwan
[c] Faculty of Engineering and Architecture, Ghent University, Belgium

ARTICLE INFO

Keywords:
Skin tribology
Tactile friction
Texture

ABSTRACT

Finger pad friction varies significantly between individuals due to personal differences and environmental effects. For this reason, comparison of the absolute friction values becomes non-informative and is rarely reported in literature. This work investigates whether friction data can be normalised to correlate between individuals. A set of textured samples were tested by 10 volunteers in dry sliding conditions with a range of normal loads up to 4 N. A reference smooth sample was used for each participant to normalise the dataset. The proposed approach allows to eliminate one of the unknown parameters, e.g., finger pad ridge contact area function, and discuss the data with respect to other variables.

1. Introduction

The physical properties of a product surface can be perceived by humans through active touch and tactile exploration of the surface by the finger pad. An important requirement for texture discrimination is a relative sliding movement between the finger pad and a surface [1]. Resulting friction and normal forces serve as a stimulus, which activate groups of mechanoreceptors located just below the skin surface. Surface textures can be designed to modify this frictional behaviour with the aim to enhance the product tactile perception or improve its handling performance by making it more sticky or slippery. For research and development purposes texture design might be validated by friction experiments. The experimental data could, however, easily result to a very broad set of friction values when compared between individuals [2–4]. The variance is partially caused by change in the operational conditions and partially by differences in the finger pad structure from person to person. Therefore, it is not possible to compare finger pad friction data quantitatively between studies, nor to validate texture designs in a generic way based on friction experiments involving multiple persons. Normalisation of the finger pad friction could allow to compare those results and evaluate the contact conditions at the scale of the finger pad – texture interaction.

Contact with a finger pad depends on phenomena occurring at multiple length scales. On the macro scale the finger pad deforms producing a near-elliptical shaped gross contact A_g. As suggested by conventional Hertzian model [5], gross contact area is expected to increase with the normal load to the power of 2/3. However, experimental results show that gross contact area follows a power function of the normal load $A_g = k \cdot F^m$ with the reported exponents m ranging from 0.1 to 0.5 [6–9], suggesting the influence of other parameters. Naturally, people have a different size of the fingertip and, therefore, the finger pad radius differs from person to person. Moreover, the inclination of the finger relative to the surface influences the resulting fingertip radius. Dzidek et al. [8] measured the finger pad gross contact areas at angles of 30 and 45 degrees to the surface. Best power function fits maintained similar exponents $m \approx 0.36$, while the reduction in contact area was associated with a decrease in coefficient k. Another influencing parameter, the effective elastic modulus of the skin, is related to finger deformation. At low normal loads, the gross contact area is restricted by harder outer skin layers, while at higher loads, finger pad deformation is restrained by the *distal phalanx* bone [6,8].

At the meso scale, the finger pad – surface interaction involves deformation of the fingerprint ridges, which form a characteristically shaped contact region. Hereinafter it is also referred to as a ridge contact area. A fingerprint structure has an approximate spacing of 350–600 μm between the ridges with respective heights of 40–100 μm [7,10–12]. Ridge contact area is often assumed to represent the real contact area in contact with smooth flat surfaces [9,13,14]. It remains a fraction of the gross contact area with reported values between 0.1 and 0.7 depending on the normal load [3,9,12,13]. Ridge contact area follows a similar power function as gross contact i.e., $A_{fr} = k \cdot F^m$, but with a different coefficient and exponent. The exponents reported in literature are generally higher that those calculated for the gross contact and vary

* Corresponding author.
E-mail address: d.sergachev@utwente.nl (D.A. Sergachev).

https://doi.org/10.1016/j.triboint.2021.107052
Received 19 January 2021; Received in revised form 8 April 2021; Accepted 11 April 2021
Available online 20 April 2021

Nomenclature

A_{fr}	contact area of fingerprint ridges (m^2)
A_g	gross contact area of a finger pad (m^2)
A_r	real contact area (m^2)
A_{rref}	real contact area of a finger pad with a reference sample (m^2)
F	applied normal load (N)
F_{adh}	interfacial adhesion friction force (N)
$F_{f\,ref}$	friction force, measured against reference sample (N)
$F_{f\,tex}$	friction force, measured against a textured sample (N)
k	power-law coefficient for contact area (m^2N^{-m})
m	power-law load index for contact area (-)
p_r	mean real contact pressure (Pa)
p_{fr}	mean ridge contact pressure (Pa)
$\widehat{p}_{fr}$	mean ridge contact pressure normalised by the point of reference (-)
r	contact area ratio, calculated by normalisation (-)
r_s	contact area ratio, calculated with numerical model (-)
α	pressure coefficient (-)
μ_{ref}	friction coefficient, calculated for a reference sample (-)
μ_{tex}	friction coefficient, calculated for a textured sample (-)
τ	interfacial shear strength (Pa)
τ_0	intrinsic interfacial shear strength (Pa)

from 0.2 to 0.7 [6,8,9,15]. A few contact models were proposed for the prediction of the finger ridge contact [8,12]. However, they require skin elasticity and fingerprint topography data for the estimation.

The micro-scale is considered in this work for contact with surface features, that have smaller dimensions than the fingerprint ridge at least by one order of magnitude. In this case the ridge is supported along its width by multiple asperities and the sum of their contacts defines the real contact area. Without reliable methods to measure the real contact area, only comparative analysis can be performed, e.g. based on friction measurements with designed and deterministic textures. Given the predominantly adhesive nature of the finger pad friction [16–18], introduction of surface texture allows to reduce and limit the real contact area, which allows to study the contact mechanics on the microscale [7,12,17]. Nevertheless, to predict friction for an individual, one requires to know the contact area at meso scale, interfacial shear strength and effective elastic modulus of the skin at microscale.

Coefficient of friction is rarely compared between volunteers due to its variation based on personal and environmental differences [19,20]. Veijgen et al. [21] reported a linear relationship between corneometer hydration values and dynamic friction coefficient. Arvidsson et al. proposed to normalise the friction measurements with the moisture level from the corneometer [22]. They observed the linear increase of the friction coefficient with the rise in skin hydration level for the same sample and finger. Moreover, the data between several participants was compared after linear normalisation of the friction coefficients, based on the ratio between mean total and mean individual values.

The aim of the current work is to investigate whether tactile friction against textured surfaces can be compared between individuals after data normalisation with respect to discussed variables. This approach is designed thus to normalise finger pad friction measurements with the intention of analysing mechanistic factors in comparative studies of tactile friction. The method that is used in the current work is original for skin friction and based on experimental work that uses deterministic surface textures and a smooth reference sample.

2. Materials and methods

2.1. Materials

Surface texture designs were selected based on our previous studies [23,24] with the aim to represent three distinctive contact states, i.e., contact with asperity features, full contact with a texture valley and a gradual transition between the two. This approach allows to estimate microscale deformation based on friction measurements. Therefore, three respective textured surfaces and a non-textured reference were used in this study. All textures consist of square packed evenly distributed asperities (Fig. 1). Textures S100 and S200 have spherical asperities with a lateral spacing of 100 and 200 μm respectively. Bumps have the same tip radius of 27 μm and height of 22 μm. Sample E200 consists of ellipsoidal asperities placed with a spacing of 200 μm between each other. Ellipsoids have a minor and major lengths of 50 and 100 μm respectively. The ellipsoidal texture also had the highest feature height of 47 μm. Flat reference samples had an average roughness of 70 nm. The surface topography was obtained with a 3D LED confocal microscope S neox (Sensofar, Spain).

Textures were replicated on a silicone rubber to promote a compliant adhesive contact and prohibit a rise of the deformation friction. Samples were produced by taking a 2 mm thick imprint from a textured embossing roll with commercial silicone rubber ALPA-SIL 97071-3 (CHT Group, Germany). It has a Shore-A hardness of 45 and an estimated Young's modulus of 1.5 MPa. Silicone was cut into equal pieces of 50 × 50 mm and glued to polycarbonate mounting plates using a silicone rubber adhesive Sil-Poxy™ (Smooth-on, USA). Texture features were aligned to perform sliding parallel to the vertical direction of Fig. 1. Therefore, elliptical texture was moved along the major asperity radius to reduce deformation friction component.

Samples were wet wiped with tissues soaked in acetone and alcohol and rinsed with demineralised water. Prior to the friction measurements the samples were put in a vacuum chamber for at least 12 h to prevent possible rubber swelling.

2.2. Friction measurements

Friction measurements were performed with a setup designed by Klaassen et al. [19]. The equipment was customised for finger pad sliding tests. The instrument consists of a chamber with a lead screw driven linear stage, which carries a balancing lever with a loadcell on one end and a counterweight on the other (Fig. 2). The hand is placed on a stage palm up with an index finger positioned on a 30-degree wedge. The sample plate attached to the transducer is lowered on top of a finger pad while the normal load is set with a static weight. An additional motor was mounted on a stage to set the sensitivity drift correction, control the lever lowering speed and lock its position angle during carriage return.

Measurements were performed in-vivo with a test group of 10 adult and healthy volunteers (8 males and 2 females), represented within the ages range of 25–55. Before the experiment, the test procedure was thoroughly explained to each participant and an informed consent was taken. Each participant had his own set of four samples. Sample order was randomised and tested within the same day per person.

The tests were carried out in an ambient environment with the temperature and humidity being measured. Prior to performing measurements with each sample, a participant was asked to wash hands with a soap and air dry them for 15 min. Afterwards an index finger pad skin hydration level was taken with a Corneometer CM 825 (Courage + Khazaka GmbH, Germany). At the first load of 0.2 N three preliminary strokes were performed to form a sweat and sebum layer on the surface.

The sample was moved from a subject's body with a constant velocity of 2 mm/s and a total sliding distance of 20 mm. Initial acceleration was set to 2 mm/s^2 to ensure that it does not affect the dynamic friction. After each stroke, the sample was lifted, and the stage was

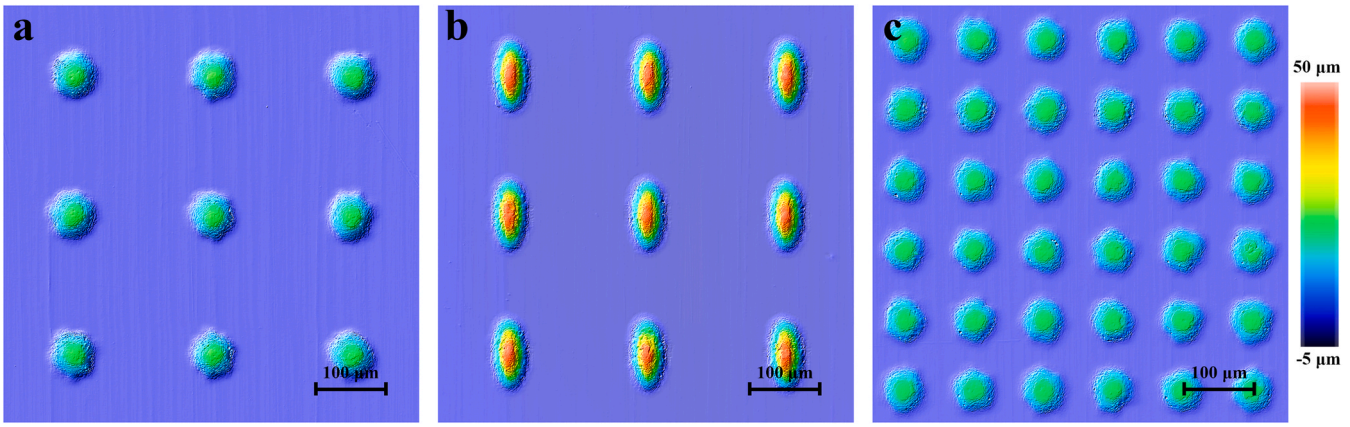

Fig. 1. Surface topography of S200 (a), E200 (b) and S100 (c) obtained with confocal microscopy.

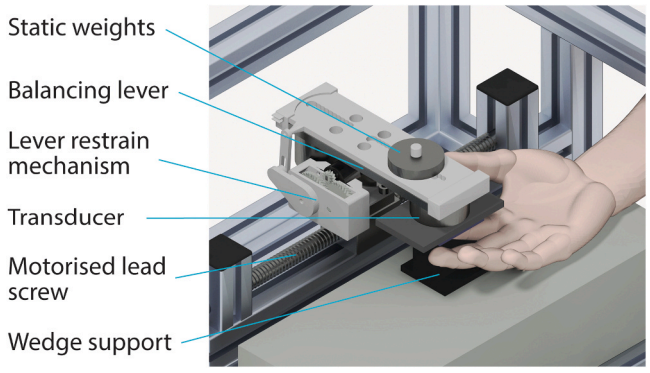

Fig. 2. Schematic representation of the test setup.

returned to its starting position.

The normal load was increased during the measurement series, starting from 0.2 N and followed by the load range from 0.5 N to 4 N with a step of 0.5 N. This decision was made to reduce the variation of the contact area due to the visco-elastic behaviour of the finger pad and conserve the time needed for full finger shape restoration. Three consecutive strokes were performed for each normal load.

2.3. Data processing

The forces were measured with a 6-axis Mini40 transducer (Schunk, Germany) at a sampling rate of 100 Hz. The load cell has a resolution of 6 mN and 2 mN in the normal and tangential directions respectively.

A MATLAB script was used to extract the forces and friction coefficient during sliding. That was performed to ensure that initial rising slope, which corresponds to the finger pad deformation, does not influence the results. A high wavelength noise of 0.5 Hz introduced by the guide bearing was removed from the signal. It is recognisable due to the pitch distance of the lead screw of 4 mm and a number of shaft revolutions per second with a chosen speed. Notably, removing of the specific wavelength does not influence the mean value, but reduces signal deviations. The data from the consecutive measurements at each normal load were used to find the arithmetic mean and standard deviation.

3. Calculation

A minimum dataset that can be used for normalisation consists of friction measurements performed for a single person at a range of normal loads. At least two tested samples are required: a textured sample of interest and a smooth surface to serve as a reference. The obtained data is represented by two friction force functions of the normal load $F_{f_{ref}}(F)$ and $F_{f_{tex}}(F)$ for the reference and the textured samples respectively.

The following assumptions are taken for further analysis:

1. Fingerprint ridge contact area A_{fr} as a function of normal load does not change for a person during the whole measurement series.
2. The real contact area with the reference sample $A_{r_{ref}}$ approaches the ridge contact area of the finger pad $A_{r_{ref}} \rightarrow A_{fr}$ at all normal loads. It implies that the roughness of the skin on the fingerprint ridges is considered negligible.
3. The deformation component of friction is small and, therefore, the friction force is based purely on adhesion, so that $F_f = F_{adh} = \tau A_r$, where τ is the interfacial shear strength and A_r is the real contact area.

With the given assumptions, the measured friction force with a flat sample can be used as a control reference. It can be approximated as a power function of the normal load as $F_{f_{ref}}(F) \approx kF^m$, where k and m are the power-law coefficient and exponent, respectively. Power law fit approximation is performed to reduce calculation errors caused by the deviation of the normal loads during measurements.

The friction data for the surface of interest can be represented as a unitless real contact area fraction. This designation is chosen instead of a neutral "normalised coefficient of friction" to emphasize the fundamental meaning behind the obtained values. Considering that the interfacial shear strength τ remains constant for the dataset, the contact area ratio r can be found as a quotient of the friction coefficients or friction forces:

$$r(F) = \frac{\mu_{tex}(F)}{\mu_{ref}(F)} = \frac{\tau A_r(F)}{\tau A_{fr}(F)} = \frac{F_{f_{tex}}(F)}{F_{f_{ref}}(F)}, \quad (1)$$

where the $F_{f_{tex}}(F)$ is the measured friction force for the textured sample and $F_{f_{ref}}(F)$ is a power fit function for the flat reference. Plotting the contact ratio against the normal load allows to evaluate contact area development and compare it between datasets.

However, with a variation of ridge contact area between individuals, the same normal load corresponds to a different ridge pressure. To compare the contact area development at the micro scale, the data can be plotted as a function of the mean ridge pressure. It cannot be found numerically without additional measurements, but it can be substituted by a ratio of the normal and tangential forces. Given that the mean ridge pressure is a function of the normal load as $p_{fr}(F) = F/A_{fr}(F)$, friction data from a reference surface can be used to obtain a dimensionless force ratio:

$$p_{fr}(F) \Big/ \tau = F \Big/ \tau A_{fr}(F) = F \Big/ F_{f\,ref}(F) \quad (2)$$

Plotting contact area ratio as a function of the force ratio $r\left(p_{fr}/\tau\right)$ removes a power component and allows to compare the micro-contact development between different persons. For the linear elastic case, deformation is linearly proportional to the applied stress. It implies that the for the same textured surface the function of $r\left(p_{fr}/\tau\right)$ is expected to vary between individuals linearly. The difference will be defined by the interfacial shear strength τ and effective Young's modulus, both can be considered unique and constant for each dataset.

Influence of the effective elastic modulus is generally removed by normalisation of the mean ridge contact pressure by effective elastic modulus or maximum pressure [12,25,26]. With those values unknown, the axis can be normalised by a p_{fr}/τ value, which corresponds to a specific contact area ratio. Use of the deterministic surfaces allows to define the value as a force ratio, at which real contact area fraction for two textures is equal. This step allows to compare experimental data with a contact model and discuss the initial assumptions.

4. Results

4.1. Environmental and corneometer measurements

Measurements with volunteers were performed at different days and times of the day. Room temperature was kept at 22 ± 0.5 °C through the measurements. Average relative humidity of 58 ± 5% was calculated across participants. Corneometer measurements however, varied significantly between individuals (Fig. 3). Most of the volunteers had skin hydration levels with the values between 40 and 60 arbitrary units (AU), which relates to a normal skin condition [27], with subjects V1 and V3 showing extreme values around 30 and 80 AU. For most of the participants skin hydration remained relatively stable during four friction measurement series with a standard deviation below 10 AU. Higher variance during the series can be noticed for V4 and V9, however no specific trend was observed.

4.2. Friction measurements

All friction tests exhibited a steady motion without a notable stick-slip effect. As anticipated, the calculated friction coefficients varied greatly between volunteers. The difference between the highest and the lowest values for the equivalent samples and normal loads reaches a factor of 4. Flat reference samples showed reduction of friction with increase of the applied normal load, reaching the range of 0.9–2.5 at 4 N (Fig. 4a). Textured samples S200 and E200 exhibited significantly lower coefficient of friction at low normal loads as observed on Fig. 4b and c. However, friction increased with the applied normal loads and stabilised in value ranges of 1.1–2.0 and 0.7–1.3 for S200 and E200 respectively. The lowest friction coefficient was observed for the highest density texture S100 and remained independent of normal load at respective values of 0.35–1.0 (Fig. 4d).

Volunteers can be arranged in descending order by the coefficient of friction for the specific texture and the normal load. However, only the order for the flat reference sample remains consistent for every normal load. The comparison between 0.5 N and 3 N normal loads is presented on Fig. 5. The sorting order for the textured samples does not follow the same trend. High friction with a reference surface for the specific volunteer does not imply that the same holds true for the textured surfaces.

4.3. Power law fit

The best power law function fit was determined for each volunteer based on the reference friction measurements from Fig. 4a. The power law equation for the coefficient of friction μ was represented as a function of normal load F as: $\mu(F) = k \cdot F^{m-1}$, where k and m are the power-law coefficient and the load index respectively [16]. Consequently, friction force can be represented as $F_{f_{ref}}(F) = k \cdot F^{m}$. The only three data points which were considered as outliers belong to V1 at 2.0 N, 2.5 N and 3.0 N and stand out from the rest of the curve (Fig. 4a), therefore they were excluded for the best fit calculation. The comparison of the found functions are provided below in the Table 1. Coefficient of determination R^2 was used to evaluate the success of the power fits and was above 0.8 for most of the curves. The exponents for the friction forces fits lay in the range from 0.58 to 0.89, while the latter was obtained from the poor fit for V9. Interestingly, the highest values for the exponent correspond to the subjects with the lowest skin hydration: V3, V6, V8.

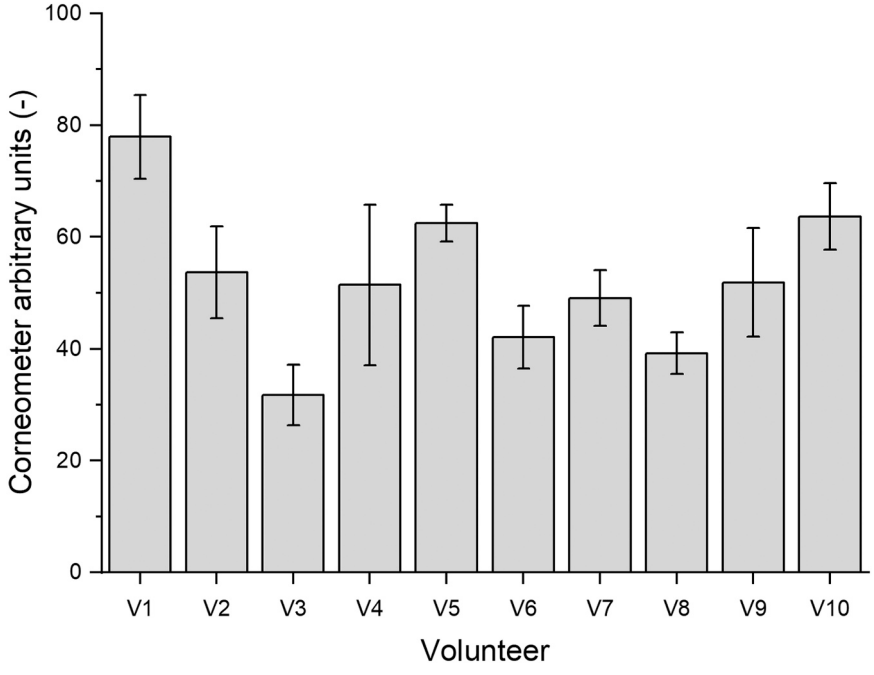

Fig. 3. Mean corneometer measurements over the test duration with standard deviation for each participant.

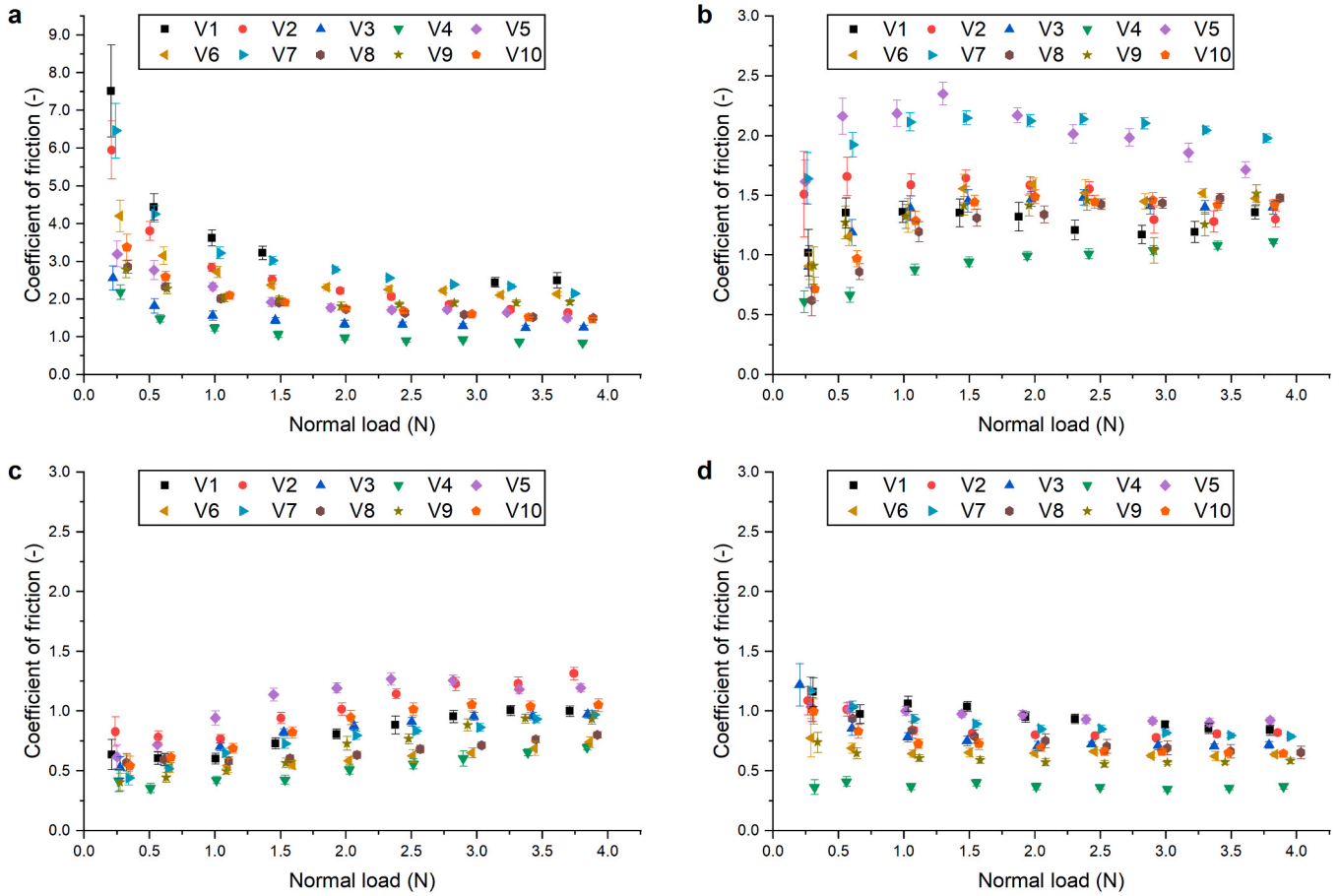

Fig. 4. Calculated coefficient of friction for all the subjects grouped by surface texture: reference(a), S200 (b), E200 (c), S100 (d). Note the different Y-scale for graph (a).

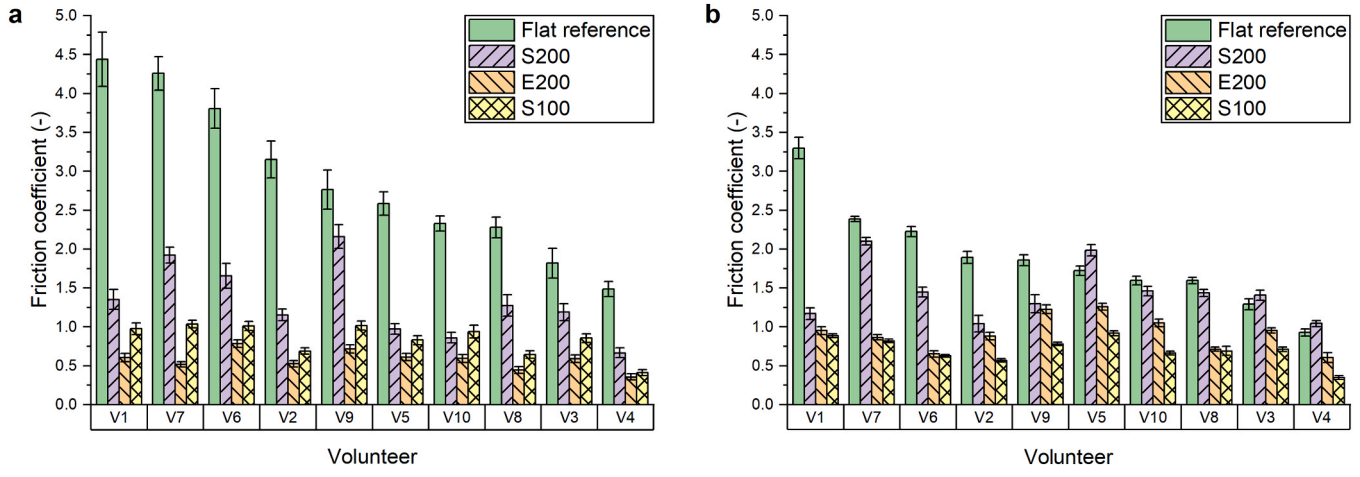

Fig. 5. Coefficient of friction for each volunteer calculated at 0.5 N (a) and 3 N (b) normal load. The data is sorted in descending order based on the measurements against the flat reference sample.

4.4. Normalisation of friction forces

Obtained power fits are used to normalise the friction data using Eq. (1). The resulted graphs are shown on Fig. 6. With this representation the influence of the interfacial shear strength is eliminated, and the contact area development can now be compared between textures and volunteers. The highest contact area ratios are shared by subjects V3, V4 and V5, who have previously shown various hydration levels and friction coefficients. For V3, who had the lowest corneometer readings, it indicates a smaller ridge contact area.

4.5. Conversion to ridge pressure

Another power function component was removed from the data by representing contact area fraction as a function of force ratio $r\left(p_{fr}/\tau\right)$

Table 1
Power fit functions for the friction force measured against the reference sample and coefficient of determination. Failed power fit for V9 marked in italic.

	V1	V2	V3	V4	V5
Friction force fit function, F_f	$3.64F^{0.66}$	$2.89F^{0.58}$	$1.60F^{0.79}$	$1.27F^{0.68}$	$2.23F^{0.72}$
Coefficient of determination, R^2	0.96	0.99	0.91	0.94	0.94
	V6	V7	V8	*V9*	V10
Friction force fit function, F_f	$2.70F^{0.79}$	$3.45F^{0.65}$	$2.08F^{0.75}$	$2.12F^{0.89}$	$2.21F^{0.69}$
Coefficient of determination, R^2	0.85	0.98	0.98	*0.61*	0.98

according to the Eq. (2). After plotting the graphs, the change of the trend for the texture E200 shown on Fig. 7b became evident for all volunteers. It consists of two parts: initial slope comparable to results of S100 on Fig. 7c and subsequent change of inclination similar to S200 Fig. 7a. On the contrary, surface S100 has a linear trend for all participants. Normalised data for texture S200 show the largest variation. Volunteers V3, V4 and V5 have a calculated real contact ratio above 1 (Fig. 7a), which contradicts the second initial assumption. Interestingly, for two of these participants, V3 and V5, the contact area growth rate decreases around the value of 1.2.

5. Discussion

5.1. General

Direct comparison of the absolute friction values between volunteers provides little insight about the origin of the observed differences. Contact conditions for each person differ based on their unique index finger pad structure and skin properties [8]. Even if friction measurements are performed at the same normal load on the macro-scale, at the asperity level the ridge contact pressure differs, as it remains inversely proportional to each individual's ridge contact area. Furthermore, interfacial shear strength cannot be considered constant for all volunteers. The values reported in literature vary between 1 kPa and 1.2 MPa for various anatomical locations and materials in contact [4,28–30].

In this work comparison of the friction results between volunteers is performed by utilising designed deterministic surfaces [24]. The contact with the textured surfaces can be divided in general, into three distinctive stages. At low normal loads, the skin is fully supported by asperities resulting in a reduced real contact area. With increase of the normal load, the skin micro-deformation exceeds the texture height and comes in contact with the lower surface. This increases the real area of contact and ultimately leads to a transition from the asperity contact state to full contact. This transition is characterised by an increase in friction coefficient. Finally, the contact stabilises at full contact state and further rise of the contact area becomes negligible. The effect of contact transition was discussed by other researchers [7,12,31] and an approach to model it was proposed in our previous work [23].

All three contact states are observed for the textured surfaces. Textures S200 and E200 display an increase in friction coefficient as skin deforms and comes in a contact with a texture valley (Fig. 4b, c). Elliptic texture E200 has a higher equivalent asperity radius and height, therefore, it can support higher load before contact transition starts. It also showed the lowest coefficient of friction across all subjects at normal loads below 1 N. That confirms the initial asperity contact state, considering that the feature density for E200 texture is lower than that

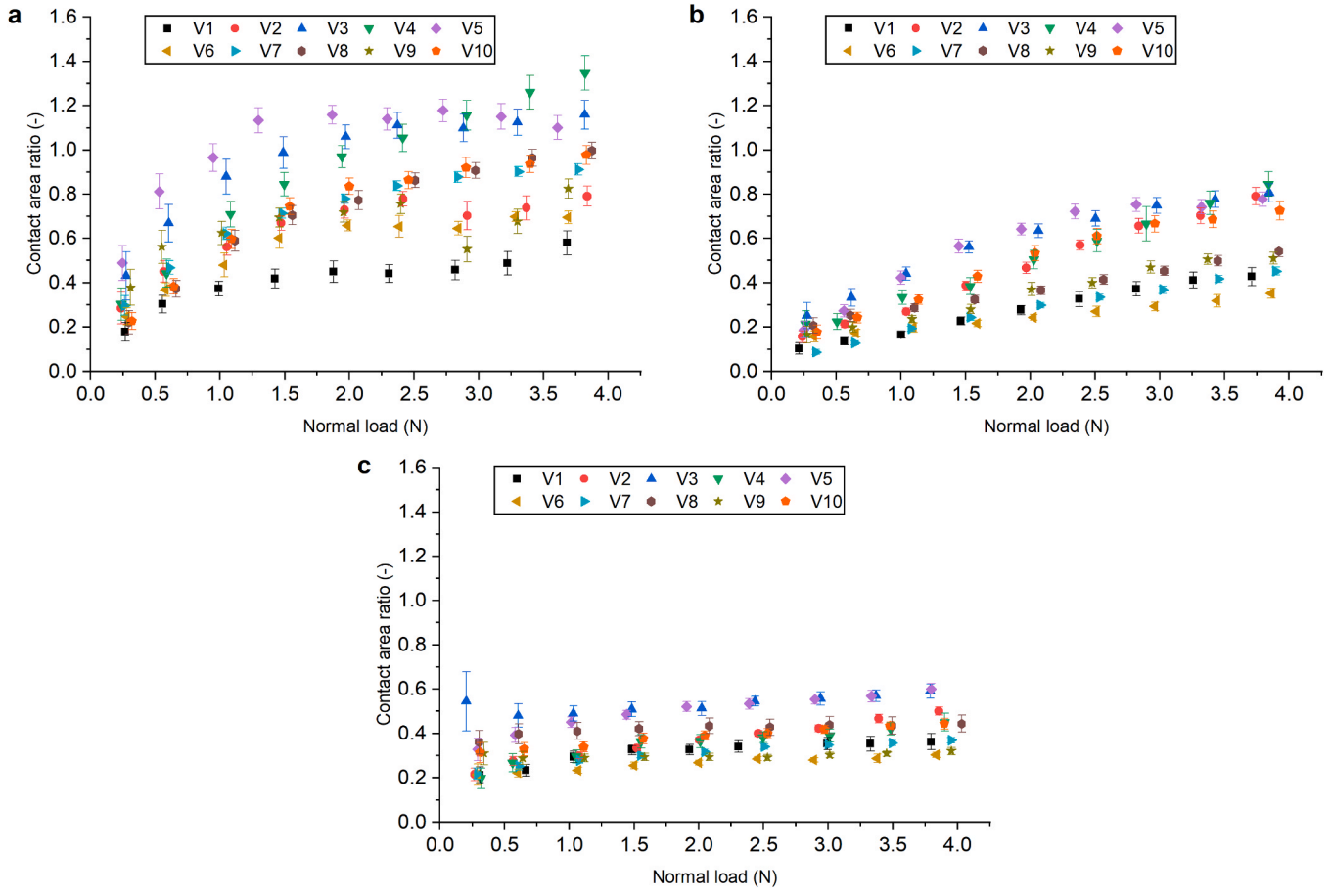

Fig. 6. Calculated contact area ratio as a function of normal load grouped by texture: S200 (a), E200 (b), S100 (c).

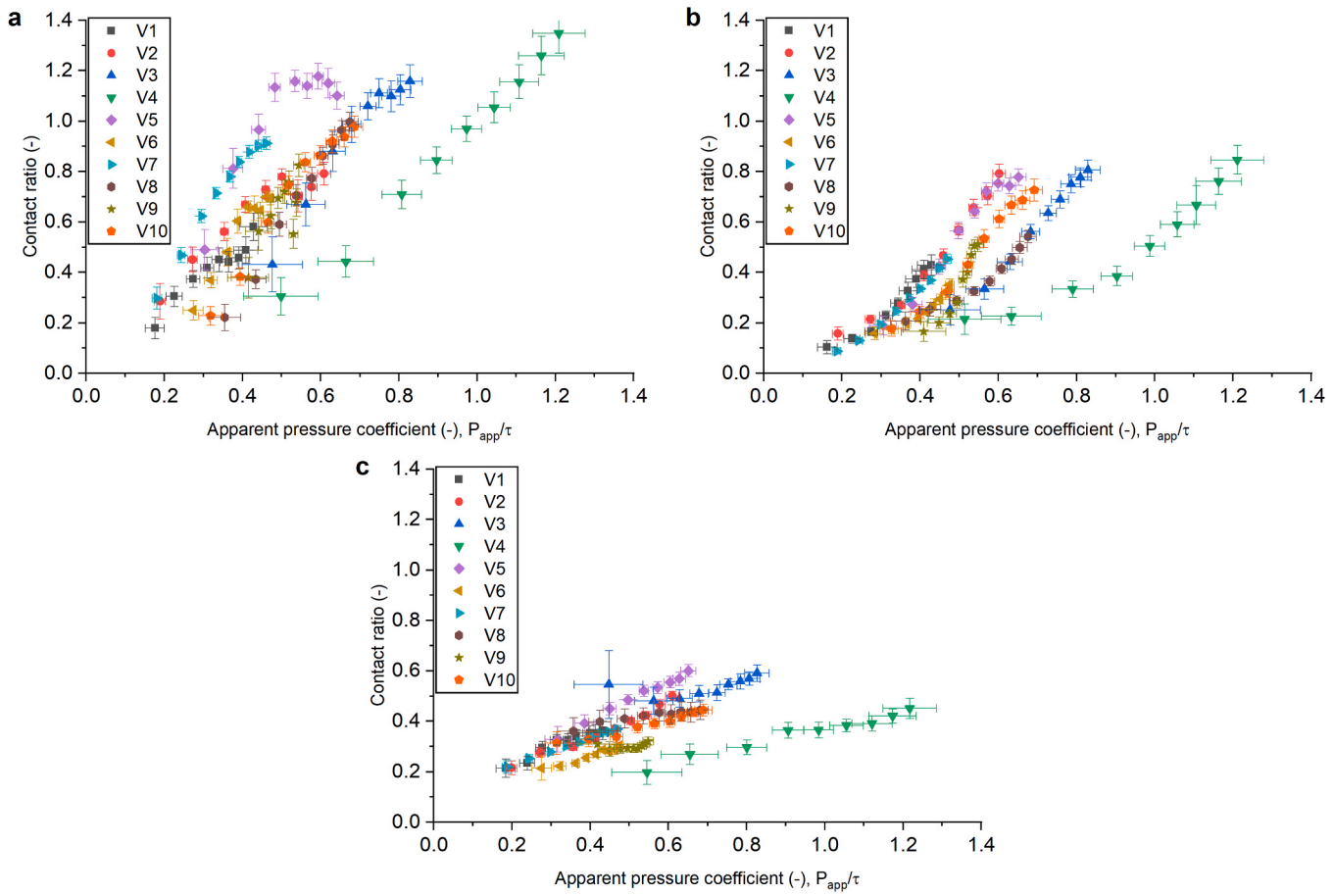

Fig. 7. Calculated contact area ratio as a function of pressure ratio grouped by texture: S200 (a), E200 (b), S100 (c).

for S100. High density texture S100 remains in asperity contact for all volunteers, which is represented in consistently low friction coefficient across all normal loads (Fig. 4d). The difference between samples is depicted on Fig. 8 for a single volunteer. Interestingly, the texture related trends are independent from the volunteer that tested the samples and can be described in a similar way.

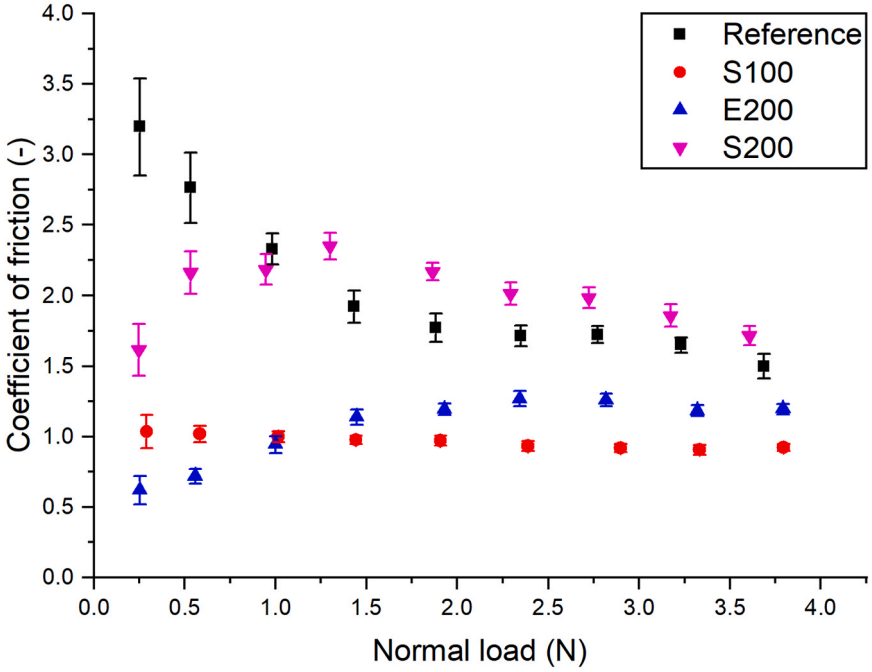

Fig. 8. Calculated coefficient of friction for the 4 surfaces tested by volunteer V5.

5.2. Reference value for normalisation

The validity of using a reference sample for normalisation can be judged by examining the results for the textured surfaces E200 and S100 more closely. E200 showed the lowest coefficient of friction for all participants at normal loads below 1 N. However, at higher loads, friction increased due to the transition to full contact state. The trends for the two textured surfaces E200 and S100 can be compared to estimate a point of intersection, at which friction coefficient and, therefore, contact area ratio become equal for those surfaces. On Fig. 8 such intersection can be observed at 1 N normal load. On the normalised graph this point should correspond to the same contact area ratio value for all participants.

For the linear elastic case, the intersection of those functions corresponds to a specific deformation. Fig. 9 shows the matching values for two volunteers, at which friction coefficient and, therefore, contact area ratio becomes equal for those surfaces. Due to the differences in ridge contact area and elastic modulus of the skin, normal load at those points significantly vary between volunteers. Table 2 represents the values for the equivalent point for each participant. The mean contact area fraction for the volunteers averages at 0.37. However, participants V3, V5 and V8 deviate further from the rest with the values above 0.43.

The high deviation from other results for these participants indicates a contradiction to the taken assumptions. Therefore, normalisation of their data could be unrepresentative. Interestingly, both volunteers V3 and V8 showed the lowest skin hydration values. Moreover, participants V3 and V5 showed contact area ratio larger than 1 on Fig. 7a. This is a probable case if those volunteers had high fingerprint ridge roughness which led to a reduced contact area with a reference sample.

5.3. Normalisation by the point of reference

Considering that a linear elastic case can be applied for small skin deformations, each dataset is normalised by the intersection point discussed above, which corresponds to a mean contact ratio value of 0.37. This point of intersection can be clearly defined both for the friction results and a contact model, which allows to apply the same normalisation approach and oppose the assumptions. This operation allows to eliminate the remaining personal differences from the graphs on Fig. 7.

Table 2
Normal loads at which contact area ratio for two surfaces S100 and E200 becomes equal.

	V1	V2	V3	V4	V5
Contact area ratio, r [-]	0.35	0.31	0.50	0.35	0.46
Normal load, F [N]	2.57	1.19	1.27	1.27	1.12
	V6	V7	V8	V9	V10
Contact area ratio, r [-]	0.28	0.34	0.43	0.29	0.35
Normal load, F [N]	2.74	2.65	2.79	1.61	1.25

The convergence of the data for the textured surfaces E200 and S100 means that deformation on the asperity scale remains proportional to pressure for all volunteers. Notably, on Fig. 10c volunteers V3, V5 and V8 show higher values than other participants. As discussed above, skin roughness and low skin hydration resulted in reduced friction against reference samples introducing error to the normalised results.

5.4. Comparison with numerical model

A boundary element method (BEM) was used to calculate a contact area ratio for a micro-scale case. The contact was assumed as a half-space linear elastic problem. Skin was assumed ideally flat, while the texture topography was obtained from confocal measurements. Contact area ratio can be plotted against normalised pressure to represent a function of surface topography. In this case effective elastic modulus chosen for the simulation becomes irrelevant. Normally ridge pressure is normalised by the Young's modulus or pressure at maximum contact. To compare the model with experimental results the data is normalised by the point of intersection for two textures E200 and S100.

After the normalisation of pressure, the total deformation range can be compared to experimental results on Fig. 11. The modelled results are fit to the frictional data as $r\left(\widehat{p}_{fr}\right) = r_s\left(\widehat{p}_{fr}\right) + 0.2\widehat{p}_{fr}$, where $r_s\left(\widehat{p}_{fr}\right)$ is a contact area ratio function obtained from the numerical model and $\widehat{p}_{fr}$ is a mean ridge contact pressure normalised by the reference point. Interestingly, the linear fit does not change with texture or participant. It suggests that coefficient of friction is proportional to pressure. This behaviour is best explained by the interfacial shear strength relation to pressure proposed by Adams et al. [28]. They proposed that in the

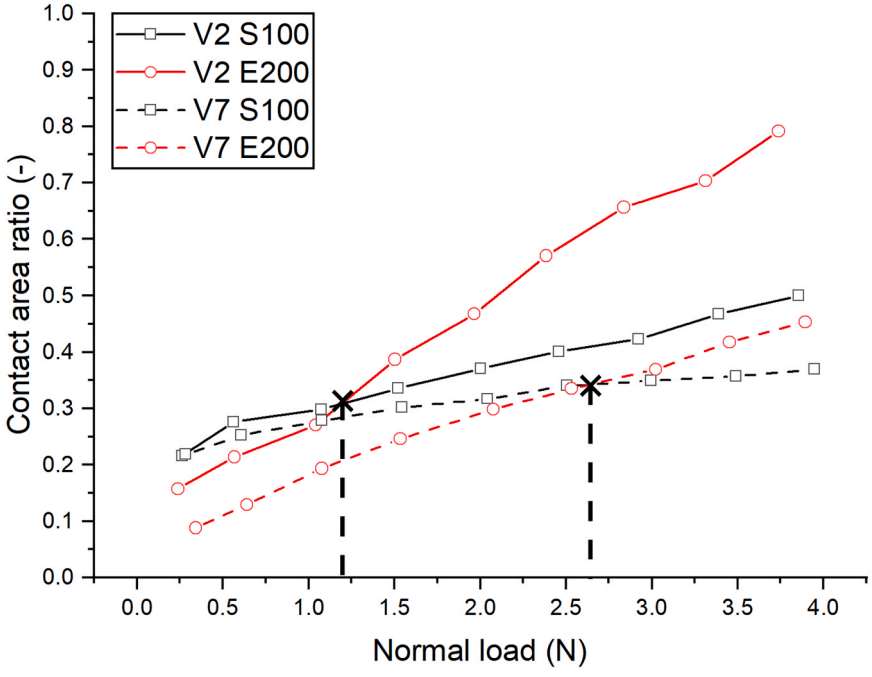

Fig. 9. Intersection of the calculated contact area ratio trends for textures S100 and E200.

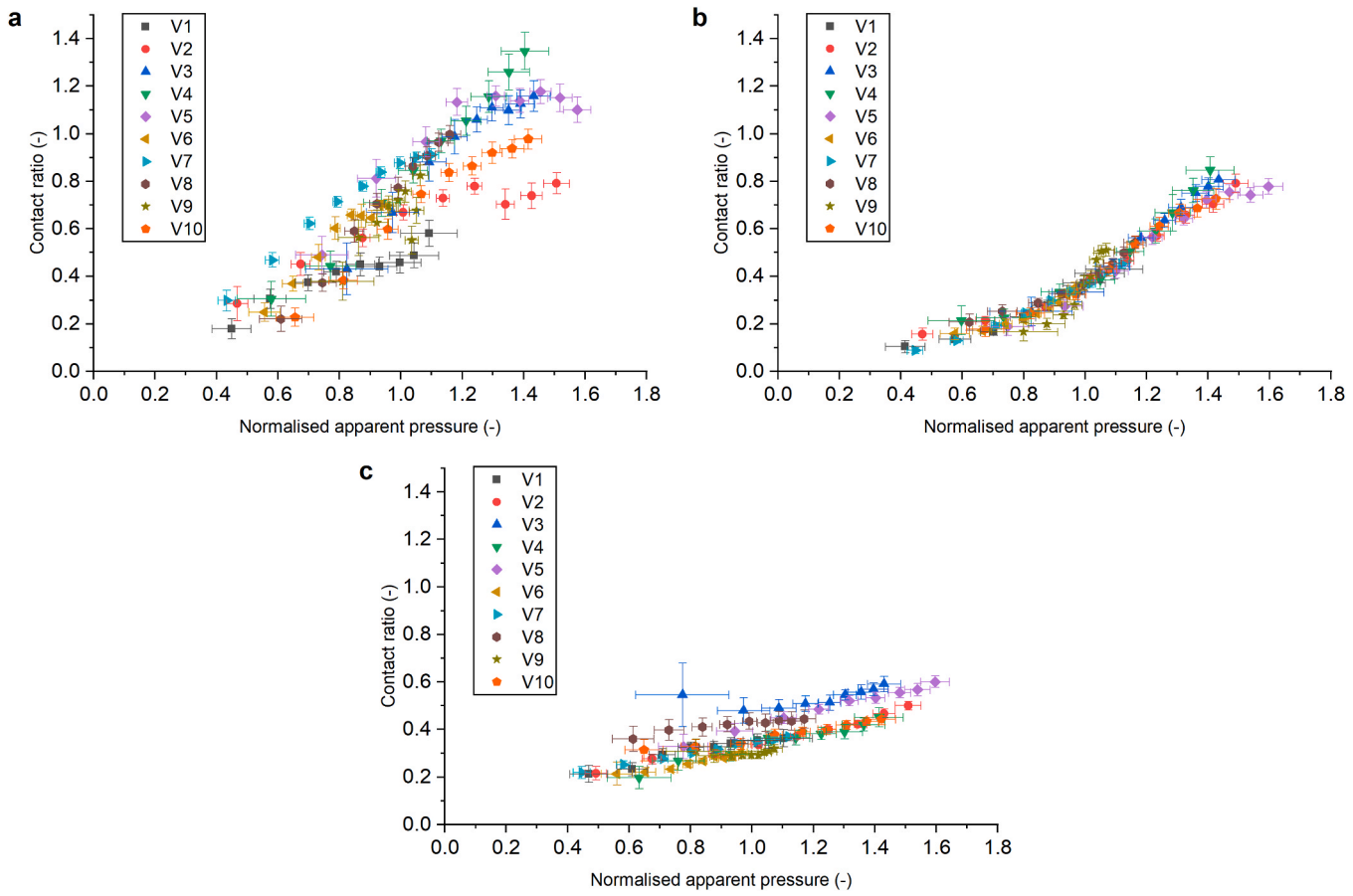

Fig. 10. Calculated contact area ratio as a function of normalised pressure grouped by texture: S200 (a), E200 (b), S100 (c).

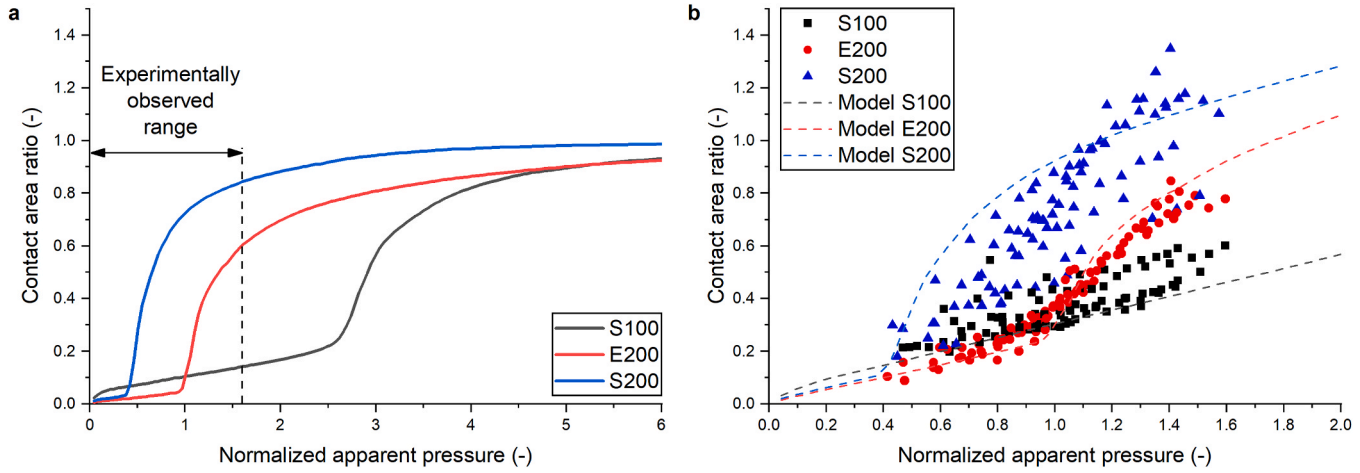

Fig. 11. Contact model results for textured surfaces (a) and its fit to the normalised friction data (b).

presence of a thin organic film, such as sebum layer, the interfacial shear strength τ is not a constant, but a linear function of the real contact pressure p_r as follows: $\tau = \tau_0 + \alpha p_r$, where τ_0 is the intrinsic interfacial shear strength and α is a pressure coefficient. For textured surfaces average real contact pressure is expected to be several times higher, which leads to higher interfacial shear strength for the same normal load.

Interestingly, the volunteer data lies within a small range of normalised ridge pressure values. The participants experienced a similar range of skin micro-deformations, even though the personal differences were prominent. For this to hold true, the higher skin elastic modulus must be accompanied by a corresponding increase in ridge pressure and vice versa, which can be achieved by the deformation of fingerprint ridges. This could explain why perception of surface textures is closely related to texture dimensions and similar textures receive uniform ratings [32,33].

5.5. *Assumptions and limitations*

The validity of the assumptions taken in Section 3 can be discussed

based on the observed datasets. The first assumption states that fingerprint ridge contact area as a function of normal load does not change during the test series for a given individual. Environmental conditions remained stable during each test series, and measurements were performed at least 15 min after the hands cleaning procedure, which is in agreement with literature. Acclimatisation time between 10 and 30 min is considered sufficient for the skin to reach a steady state [4,19,34–36]. Based on results obtained, a change in the ridge contact area function occurred for participant V9. It was represented in a deviation of corneometer readings prior to the test with E200 and resulted in a noticeable divergence from the general trend (Fig. 7b). For most of the volunteers the skin hydration level remained stable during the measurement procedure. However, one should exercise caution if the experiments are performed across several days.

The second assumption states that real contact area for a reference sample approaches ridge contact area at all normal loads. It can be considered viable if skin and surface roughness is negligible or at least one of the surfaces is compliant. In the current study, the combination of silicone rubber material with a relatively low surface average roughness allows to satisfy the assumption. Power law fit exponents are close to the theoretical exponent of 2/3, predicted for adhesive contact and experimental values from other studies [6,13,28,37]. With increase of the reduced Young's modulus or surface roughness, real contact area reduces leading to errors during normalisation procedure as it was observed with the participants V3, V5 and V8.

The third assumption considers that the friction force is based purely on adhesion. For the dry finger pad sliding against smooth surfaces, adhesion is considered to be a predominant component of friction [16–18]. Tomlinson et al. [38] reported a 10% deformation term for the triangular ridged surfaces with the heights over 250 μm. Moreover, they found an interlocking term to become considerable for surfaces with heights above 40 μm. Textures used in this study were designed to minimise interlocking and have smaller feature sizes. However, the interfacial shear strength seems to be dependent on pressure as discussed by Adams et al. [28]. It leads to overestimation of contact area fraction after normalisation, which increases linearly with pressure and does not change with participant.

6. Conclusions

- Normalisation of the frictional data allows to reduce one of the unknown personal variables: function of the ridge contact area, reduced Young's modulus or interfacial shear strength. Furthermore, the results can be normalised to dimensionless values to compare the contact area development on the microscale. The resulted graphs confirm interfacial shear strength relation to contact pressure.
- All subjects experienced the same contact states with the tested textures, despite the personal differences, contact area and skin hydration levels.
- This suggests that deformation of the skin on the microscale is independent of the skin elasticity due to the fingerprint ridge pattern. In other words, the change of the skin Young's modulus is closely related to the reduction of the ridge contact area and, therefore, increase of the ridge pressure, leading to comparable displacement values.

Ethics approval and consent to participate

The procedures performed in the current study were approved by the Natural Sciences and Engineering Sciences Ethics committee, University of Twente, Enschede. The measurements were carried out in compliance with COVID19 government regulations active during that time.

All subjects provided a written informed consent. None of the experiments were invasive or harmful physiologically or psychologically. All data was stored anonymously, and the participants had the right to quit at any time if they so wished.

CRediT authorship contribution statement

Dmitrii Aleksandrovich Sergachev: Conceptualization, Methodology, Investigation, Formal analysis, Writing – original draft. **David Thomas Allan Matthews:** Conceptualization, Writing - review & editing, Supervision. **Emile van der Heide:** Writing - review & editing, Supervision, Funding acquisition.

Declaration of Competing Interest

The authors declare that they have no known competing financial interests or personal relationships that could have appeared to influence the work reported in this paper.

Acknowledgements

This work was supported by INTERREG is a European program and the project is funded by the European Union under the project number 142091.

References

[1] Lamb GD. Tactile discrimination of textured surfaces: psychophysical performance measurements in humans. J Physiol 1983;338:551–65. https://doi.org/10.1113/jphysiol.1983.sp014689.
[2] Veijgen NK, van der Heide E, Masen MA. A multivariable model for predicting the frictional behaviour and hydration of the human skin. Ski Res Technol 2013;19:330–8. https://doi.org/10.1111/srt.12053.
[3] Liu X, Lu Z, Lewis R, Carré MJ, Matcher SJ. Feasibility of using optical coherence tomography to study the influence of skin structure on finger friction. Tribol Int 2013;63:34–44. https://doi.org/10.1016/j.triboint.2012.08.020.
[4] Hendriks CP, Franklin SE. Influence of surface roughness, material and climate conditions on the friction of human skin. Tribol Lett 2010;37:361–73. https://doi.org/10.1007/s11249-009-9530-7.
[5] Johnson KL. Contact Mech 1985. https://doi.org/10.1115/1.3261297.
[6] Liu X, Carré MJ, Zhang Q, Lu Z, Matcher SJ, Lewis R. Measuring contact area in a sliding human finger-pad contact. Ski Res Technol 2018;24:31–44. https://doi.org/10.1111/srt.12387.
[7] Van Kuilenburg J, Masen MA, Van Der Heide E. The role of the skin microrelief in the contact behaviour of human skin: contact between the human finger and regular surface textures. Tribol Int 2013;65:81–90. https://doi.org/10.1016/j.triboint.2012.11.024.
[8] Dzidek BM, Adams MJ, Andrews JW, Zhang Z, Johnson SA. Contact mechanics of the human finger pad under compressive loads. J R Soc Interface 2017;14:20160935. https://doi.org/10.1098/rsif.2016.0935.
[9] Soneda T, Nakano K. Investigation of vibrotactile sensation of human fingerpads by observation of contact zones. Tribol Int 2010;43:210–7. https://doi.org/10.1016/j.triboint.2009.05.016.
[10] Adams MJ, Johnson SA, Lefèvre P, Lévesque V, Hayward V, André T, et al. Finger pad friction and its role in grip and touch. J R Soc Interface 2013;10:20120467. https://doi.org/10.1098/rsif.2012.0467.
[11] Fagiani R, Barbieri M. Modelling of finger-surface contact dynamics. Tribol Int 2014;74:130–7. https://doi.org/10.1016/j.triboint.2014.02.018.
[12] Rodriguez Urribarri AC, van der Heide E, Zeng X, de Rooij MB, Rodríguez Urribarrí AC, van der Heide E, et al. Modelling the static contact between a fingertip and a rigid wavy surface. Tribol Int 2016;102:114–24. https://doi.org/10.1016/j.triboint.2016.05.028.
[13] Childs THC, Henson B. Human tactile perception of screen-printed surfaces: self-report and contact mechanics experiments. Proc Inst Mech Eng Part J J Eng Tribol 2007;221:427–41. https://doi.org/10.1243/13506501JET217.
[14] Sahli R, Pallares G, Ducottet C, Ben Ali IE, Al Akhrass S, Guibert M, et al. Evolution of real contact area under shear and the value of static friction of soft materials. Proc Natl Acad Sci 2018;115:471–6. https://doi.org/10.1073/pnas.1706434115.
[15] Lin HT, Hong TF, Li WL. Grip performance affected by water-induced wrinkling of fingers. Tribol Lett 2015;58:1–9. https://doi.org/10.1007/s11249-015-0515-4.
[16] Derler S, Gerhardt LC, Lenz A, Bertaux E, Hadad M. Friction of human skin against smooth and rough glass as a function of the contact pressure. Tribol Int 2009;42:1565–74. https://doi.org/10.1016/j.triboint.2008.11.009.
[17] Duvefelt K, Olofsson U, Johannesson CM, Skedung L. Model for contact between finger and sinusoidal plane to evaluate adhesion and deformation component of friction. Tribol Int 2016;96:389–94. https://doi.org/10.1016/j.triboint.2014.12.020.
[18] Derler S, Rotaru GM. Stick-slip phenomena in the friction of human skin. Wear 2013;301:324–9. https://doi.org/10.1016/j.wear.2012.11.030.
[19] Klaassen M, Schipper DJ, Masen MA. Influence of the relative humidity and the temperature on the in-vivo friction behaviour of human skin. Biotribology 2016;6:21–8. https://doi.org/10.1016/j.biotri.2016.03.003.

[20] Veijgen NK, Masen MA, van der Heide E. Variables influencing the frictional behaviour of in vivo human skin. J Mech Behav Biomed Mater 2013;28:448–61. https://doi.org/10.1016/j.jmbbm.2013.02.009.
[21] Veijgen NK, Masen MA, Van Der Heide E. Relating friction on the human skin to the hydration and temperature of the skin. Tribol Lett 2013;49:251–62. https://doi.org/10.1007/s11249-012-0062-1.
[22] Arvidsson M, Ringstad L, Skedung L, Duvefelt K, Rutland MW. Feeling fine - the effect of topography and friction on perceived roughness and slipperiness. Biotribology 2017;11:92–101. https://doi.org/10.1016/j.biotri.2017.01.002.
[23] Sergachev DA, Matthews DTA, van der Heide E. An empirical approach for the determination of skin elasticity: finger pad friction against textured surfaces. Biotribology 2019;18:100097. https://doi.org/10.1016/j.biotri.2019.100097.
[24] Sergachev, DA, Matthews, DTA, van der Heide, E. Des bidirectional Fricti Behav Tactile Contact Using Ellipsoidal Asperity Micro-Textures, 2021.
[25] Jackson RL, Green I. On the modeling of elastic contact between rough surfaces. Tribol Trans 2011;54:300–14. https://doi.org/10.1080/10402004.2010.542277.
[26] Yastrebov VA, Anciaux G, Molinari JF. From infinitesimal to full contact between rough surfaces: evolution of the contact area. Int J Solids Struct 2015;52:83–102. https://doi.org/10.1016/j.ijsolstr.2014.09.019.
[27] Heinrich U, Koop U, Leneveu-Duchemin MC, Osterrieder K, Bielfeldt S, Chkarnat C, et al. Multicentre comparison of skin hydration in terms of physical-, physiological- and product-dependent parameters by the capacitive method (Corneometer CM 825). Int J Cosmet Sci 2003;25:45–53. https://doi.org/10.1046/j.1467-2494.2003.00172.x.
[28] Adams MJ, Briscoe BJ, Johnson SA. Friction and lubrication of human skin. Tribol Lett 2007;26:239–53. https://doi.org/10.1007/s11249-007-9206-0.
[29] Bochereau S, Dzidek B, Adams M, Hayward V. Characterizing and imaging gross and real finger contacts under dynamic loading. IEEE Trans Haptics 2017;10:456–66. https://doi.org/10.1109/TOH.2017.2686849.
[30] Derler S, Rotaru G-MM, Ke W, El Issawi-Frischknecht L, Kellenberger P, Scheel-Sailer A, et al. Microscopic contact area and friction between medical textiles and skin. J Mech Behav Biomed Mater 2014;38:114–25. https://doi.org/10.1016/j.jmbbm.2014.06.014.
[31] Zhang S, Rodriguez Urribarri A, Morales Hurtado M, Zeng X, Van Der Heide E. The role of the sliding direction against a grooved channel texture on tool steel: an experimental study on tactile friction. Int J Solids Struct 2015;56:53–61. https://doi.org/10.1016/j.ijsolstr.2014.12.005.
[32] Massimiani V, Weiland B, Chatelet E, Cornuault PH, Faucheu J, Massi F. The role of mechanical stimuli on hedonistic and topographical discrimination of textures. Tribol Int 2020;143:106082. https://doi.org/10.1016/j.triboint.2019.106082.
[33] Faucheu J, Weiland B, Juganaru-Mathieu M, Witt A, Cornuault PH. Tactile aesthetics: textures that we like or hate to touch. Acta Psychol 2019;201:102950. https://doi.org/10.1016/j.actpsy.2019.102950.
[34] Geerligs M, van Breemen L, Peters G, Ackermans P, Baaijens F, Oomens C. In vitro indentation to determine the mechanical properties of epidermis. J Biomech 2011;44:1176–81. https://doi.org/10.1016/j.jbiomech.2011.01.015.
[35] Derler S, Preiswerk M, Rotaru GM, Kaiser JP, Rossi RM. Friction mechanisms and abrasion of the human finger pad in contact with rough surfaces. Tribol Int 2015;89:119–27. https://doi.org/10.1016/j.triboint.2014.12.023.
[36] Abdouni A, Djaghloul M, Thieulin C, Vargiolu R, Pailler-Mattei C, Zahouani H. Biophysical properties of the human finger for touch comprehension: influences of ageing and gender. R Soc Open Sci 2017;4:170321. https://doi.org/10.1098/rsos.170321.
[37] Darden MA, Schwartz CJ. Investigation of friction mechanisms during the sliding of elastomers against hard parallel-ridge textures. Tribol Int 2013;63:2–7. https://doi.org/10.1016/j.triboint.2012.01.005.
[38] Tomlinson SE, Carré MJ, Lewis R, Franklin SE. Human finger contact with small, triangular ridged surfaces. Wear 2011;271:2346–53. https://doi.org/10.1016/j.wear.2010.12.055.